Letter Vol. 46, No. 13 / 1 July 2021 / Optics Letters 3083

Optics Letters

Characterization of vacuum and deep ultraviolet pulses via two-photon autocorrelation signals

S. Walker,* R. Reiff, A. Jaron-Becker, and A. Becker

JILA and Department of Physics, University of Colorado, Boulder, Colorado 80309-0440, USA
*Corresponding author: spencer.walker@colorado.edu

Received 6 April 2021; revised 13 May 2021; accepted 2 June 2021; posted 2 June 2021 (Doc. ID 427200); published 22 June 2021

Characterization of ultrashort vacuum and deep ultraviolet pulses is important in view of applications of those pulses for spectroscopic and dynamical imaging of atoms, molecules, and materials. We present an extension of the autocorrelation technique, applied for measurement of the pulse duration via a single Gaussian function. Analytic solutions for two-photon ionization of atoms by Gaussian pulses are used along with an expansion of the pulse to be characterized using multiple Gaussians at multi-color central frequencies. This approach allows one to use two-photon autocorrelation signals to characterize isolated ultrashort pulses and pulse trains, i.e., the time-dependent amplitude and phase variation of the electric field. The potential of the method is demonstrated using vacuum and deep ultraviolet pulses and pulse trains obtained from numerical simulations of macroscopic high harmonic spectra.

https://doi.org/10.1364/OL.427200

The generation of ultrashort vacuum ultraviolet (VUV) and deep ultraviolet (DUV) laser pulses [1–3] is important since excitation and ionization energies of many atoms, molecules, nanoparticles, and materials lie in this spectral region. Such laser sources are used to trigger, steer, probe, and image physical processes and chemical reactions on the ultrafast time scale, down to the attosecond regime [4–12]. Temporal pulse characterization is often required to enable the analysis of the spectroscopic data. Many ultrashort pulse characterization methods rely on the measurement of ions or photoelectrons via the autocorrelation or cross-correlation approach (for an overview, see [13]). In cross-correlation methods, the pulse to be characterized is used in superposition with a well-characterized infrared pulse [14–19], while for autocorrelation measurements, two replicas of the unknown pulse are used [20–24].

In an autocorrelation measurement, ion signals are recorded as a function of the time delay between the two replicas of the pulse. Generalized two-photon ionization cross sections for the interaction of a single Gaussian pulse with the target are then used to fit the autocorrelation trace and determine the pulse duration. This powerful method has been applied to estimate the duration of attosecond extreme ultraviolet (XUV) pulses [20,24], VUV, and DUV pulses [1,23]. The application of current pulse characterization techniques in the VUV and DUV spectral regions is limited, since many methods, such as the reconstruction of attosecond beating by interference of two-photon transitions (RABBITT) [14] or attosecond streaking technique [15], rely on the ionization of the target by absorption of a single photon from the unknown pulse.

In this work, we consider an extension of the single-Gaussian autocorrelation technique, which enables the characterization of the temporal pulse envelope of an isolated ultrashort VUV pulse or a pulse train, i.e., the time-dependent amplitude and phase variation of the electric field. The extension is based on the analytical solution to the time-dependent Schrödinger equation (TDSE) for the perturbative two-photon ionization of an atom by a Gaussian laser pulse in the single-active-electron approximation [25]. Since the solution includes both resonant and non-resonant pathways, it can be used for the characterization of broadband pulses with photon energies in the regime of typical atomic excitation energies. The unknown pulse is approximated as a superposition of Gaussian pulses, for which the amplitudes and temporal widths are determined via fitting to the two-photon autocorrelation signal generated by the unknown laser pulse. We demonstrate this extension of the single-Gaussian autocorrelation technique via applications based on results for ultrashort VUV pulses from numerical simulations of macroscopic high harmonic generation (HHG).

For the characterization, we use that the electric field of any arbitrary pulse can be written as the real part of an expansion in a basis of multi-color Gaussian functions (Hartree atomic units are used: $e = \hbar = m = 1$ a.u.):

$$\tilde{f}(t) = |\tilde{f}(t)|e^{-i\phi(t)} = \sum_{n,j} \tilde{f}_{n,j} \exp\left[-\frac{(t-\tau_{n,j})^2}{2T_{n,j}^2} - i\omega_j t\right], \tag{1}$$

where $|\tilde{f}(t)|$ and $\phi(t)$ are the time-dependent amplitude and phase of the unknown pulse, respectively. $\tilde{f}_{n,j}$ is the complex amplitude, $\tau_{n,j}$ is a translation in time, and $T_{n,j}$ is the width of a Gaussian pulse with central frequency ω_j. In the examples below, we consider linearly polarized pulses, but the expansion can be applied to other polarizations as well.

Since each Gaussian has an independent phase factor, in the multi-Gaussian approach, the nonlinear phase accumulation $\omega(t) \equiv \frac{d\phi}{dt}$ can be determined from the interferences in the two-photon autocorrelation trace. If a large frequency variation is expected, an alternative basis of linearly chirped Gaussian functions can be utilized by substituting $T_{n,j}^{-2} \to T_{n,j}^{-2} + i\alpha_{n,j}$,

where $\alpha_{n,j}$ is an additional parameter. For all pulses considered in the present work, we have used $\alpha_{n,j}=0$ to limit the number of fitting parameters.

Next, we utilize the analytic solution of the two-photon ionization amplitude for interaction of an atom in the single-active-electron approximation with two Gaussian laser pulses:

$$\begin{aligned} a^{(2)}_{f,i}(\tau_{n_2,j_2},\tau_{n_1,j_1}) &= -\frac{\pi}{4}\tilde{f}_{n_2,j_2}\tilde{f}_{n_1,j_1}T_{n_2,j_2}T_{n_1,j_1}\sum_{E_m<0} z_{f,m}z_{m,i} \\ &\times \exp\left(-\frac{1}{2}T^2_{n_2,j_2}\Delta^2_{f,m}-\frac{1}{2}T^2_{n_1,j_1}\Delta^2_{m,i}+i\Delta_{f,m}\tau_{n_2,j_2}+i\Delta_{m,i}\tau_{n_1,j_1}\right) \\ &\times\left\{1+\mathrm{erf}\left[\frac{1}{\sqrt{2}\bar{T}}\left(\tau_{n_2,j_2}-\tau_{n_1,j_1}+i\left(T^2_{n_2,j_2}\Delta_{f,m}-T^2_{n_1,j_1}\Delta_{m,i}\right)\right)\right]\right\}. \end{aligned} \tag{2}$$

We note that Eq. (2) is a generalization of the solution for a single Gaussian pulse given in [25]. Here, $\bar{T}^2=T^2_{n_2,j_2}+T^2_{n_1,j_1}$, $\Delta_{m,i}=E_{m,i}-\omega_{j_1}$, and $\Delta_{f,m}=E_{f,m}-\omega_{j_2}$, where $E_{m,i}$ and $E_{f,m}$ are the energy differences between the field-free intermediate (m) states and the initial (i) and final (f) states, respectively. $z_{f,m}$ and $z_{m,i}$ are the transition dipole moments between the respective states, which can be obtained via various theoretical techniques for an atom. In the present applications, we restrict the sum to intermediate states with $E_m<0$. To compute $\mathrm{erf}(x+iy)$, we use a continued fraction approximation for the majority of the complex plane [26] and patch the (nonphysical) singularities near the origin with the global Padé approximation [27] and other singularities near the imaginary axis with the standard Padé approximation. Since we want to characterize ultrashort pulses with large bandwidths, we have also taken into account the one-photon ionization amplitude for interaction with the nth Gaussian pulse, which is given by

$$a^{(1)}_{f,i}(\tau_{n,j})=-i\sqrt{\frac{\pi}{2}}\tilde{f}_{n,j}T_{n,j}z_{f,i}\exp\left(-\frac{1}{2}T^2_{n,j}\Delta^2_{f,i}+i\Delta_{f,i}\tau_{n,j}\right). \tag{3}$$

The autocorrelation signal for the interaction with two replicas of the arbitrary pulse delayed by a time interval τ to each other can then be approximated by the multi-color Gaussian approach as

$$P_{N_g}(\tau)=\int_{E_f>0}\left|A^{(1)}_{f,i}(\tau)+A^{(2)}_{f,i}(\tau)\right|^2 \mathrm{d}E_f, \tag{4}$$

where the integral over E_f includes all final levels f for the one- and two-photon processes, respectively:

$$A^{(1)}_{f,i}(\tau)=\sum_n\sum_j a^{(1)}_{f,i}(\tau_{n,j})\left(1+e^{iE_{f,i}\tau}\right), \tag{5}$$

$$\begin{aligned} A^{(2)}_{f,i}(\tau) &= \sum_{n_2}\sum_{j_2}\sum_{n_1}\sum_{j_1} a^{(2)}_{f,i}(\tau_{n_2,j_2},\tau_{n_1,j_1})\left(1+e^{iE_{f,i}\tau}\right) \\ &+a^{(2)}_{f,i}(\tau_{n_2,j_2}+\tau,\tau_{n_1,j_1})e^{i\omega_{j_2}\tau}+a^{(2)}_{f,i}(\tau_{n_2,j_2},\tau_{n_1,j_1}+\tau)e^{i\omega_{j_1}\tau}. \end{aligned} \tag{6}$$

To characterize the envelope of the unknown ultrashort pulse, we introduce an objective function between the autocorrelation signal $P_{\mathrm{exact}}(\tau)$, measured with the unknown pulse, and the approximate multi-Gaussian signal $P_{N_g}(\tau)$ as

$$\mathrm{obj}_{N_g}(\tau)=\frac{|P_{\mathrm{exact}}(\tau)-P_{N_g}(\tau)|}{P_{\mathrm{exact}}(0)}, \tag{7}$$

where $P_{\mathrm{exact}}(0)$ is the maximum ionization yield for which the two replicas of the pulse perfectly overlap. For a given number of Gaussian pulses, N_g, the L^2 norm of the objective function is then minimized with respect to variation of $\tilde{f}_{n,j}$, $\tau_{n,j}$, and $T_{n,j}$ using the standard nonlinear least squares approach, where the objective function has complexity that scales as the square of the number of basis functions used. Without loss of generality, for exactly one n, j, we choose $\tilde{f}_{n,j}$ real and fix $\tau_{n,j}=0$.

To test the characterization with this multi-Gaussian approach, we obtain ultrashort pulses using results of numerical macroscopic simulations of HHG spectra [28]. Calculations of the microscopic single-atom response are performed by solving the TDSE within the dipole approximation with

$$H(t)=-\frac{1}{2}\nabla^2-\frac{1}{r}+\mathbf{E}(t)\cdot\mathbf{y}, \tag{8}$$

where $\mathbf{E}(t)$ and $\mathbf{y}$ are the electric field and polarization direction of the driving laser pulse. The wavefunction has been expanded in 30 spherical harmonics and its radial part of and the potential are discretized utilizing fourth order finite difference on a radial grid with spacing $dr=0.2$ a.u. and grid sizes up to $r_{\max}=100$ a.u. [29]. As an absorbing boundary, we use exterior complex scaling (ECS), where the edge of the grid (10%) is rotated into complex space by an angle $\eta=\pi/4$. We use the Crank–Nicolson method to propagate the wave function starting from the ground state with time step $dt=0.1$. To obtain the HHG spectra $P(\omega)=|\tilde{a}(\omega)|^2$, the dipole acceleration $a(t)$ is evaluated using the Ehrenfest theorem $a(t)=\langle-\frac{\partial}{\partial y}(-\frac{1}{r})\rangle$, and the complex harmonic response $\tilde{a}(\omega)$ is obtained by taking the Fourier transform (without windowing).

For the macroscopic radiation signal, we consider the low gas density regime, which is free from longitudinal phase-matching effects. We then follow the approach used in [30], in which the macroscopic yield is obtained as the superposition of the fields generated at different points in the medium. Application of this approach requires single-atom simulations for a large number of intensities and phase factors. In the present simulations, 5×10^5 single-atom results are used via an interpolation scheme based on 100 exact TDSE results. The success of the interpolation method has been verified elsewhere [28].

In Fig. 1(a), we show the below- and near-threshold parts of the numerical macroscopic HHG signal obtained for a gas jet of hydrogen atoms interacting with a 20-cycle, 800 nm pulse at peak intensity 4×10^{13} W/cm^2. From this spectrum, we first extract isolated ultrashort pulses by applying a Gaussian filter in the frequency domain centered about the harmonic H_0, i.e., $e^{-(H-H_0)^2/2\beta^2}$, where $\beta=0.35$ in the present work. The temporal shape of the pulse filtered about the ninth harmonic varies significantly from that of a Gaussian pulse [Fig. 1(b)]. For the application of the characterization method, we use replicas of the pulse with an intensity of 3.16×10^{11} W/cm^2 to determine the autocorrelation signal shown in Fig. 1(c). The signal is obtained by solving the TDSE for the interaction of a helium atom with the two pulses; a single-active-electron potential for the helium atom [31] is used for these calculations.

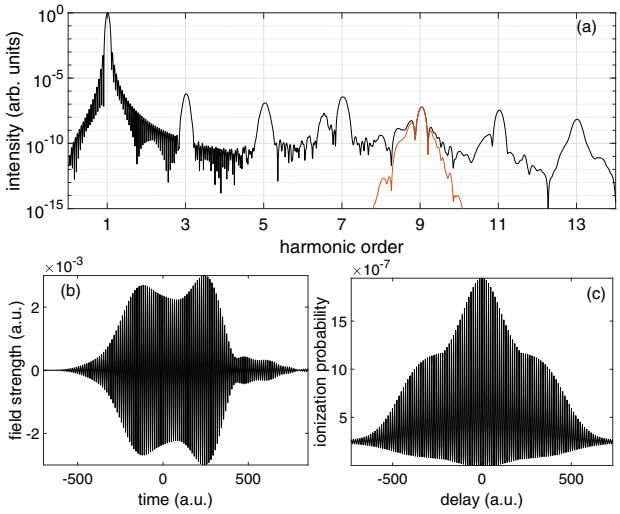

Fig. 1. (a) Macroscopic high harmonic spectrum in a hydrogen atom driven by a 20-cycle, 800 nm laser pulse at 4×10^{13} W/cm^2: full spectrum (black line) and spectrum after application of a Gaussian filter about ninth harmonic (red line). (b) Temporal profile of filtered ninth harmonic and (c) autocorrelation signal using filtered ninth harmonic.

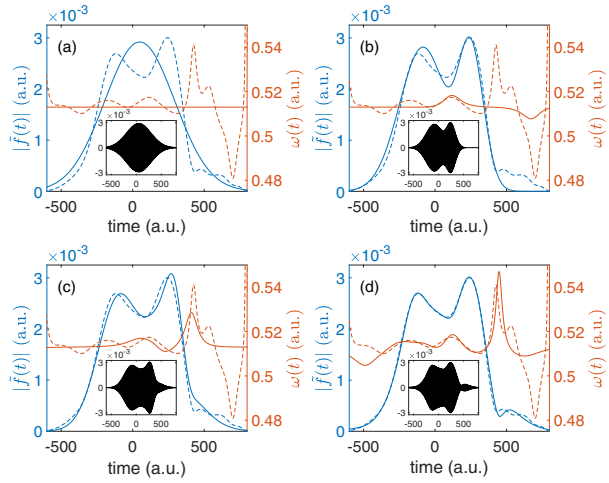

Fig. 2. Comparison of time-dependent amplitude $|\tilde{f}(t)|$ (blue line) and phase variation $\omega(t)$ (red line) of the filtered ninth harmonic (dashed line) and reconstructed pulse with (a) one, (b) two, (c) four, and (d) six Gaussians (solid line). The temporal profile is also provided as insets within each subplot.

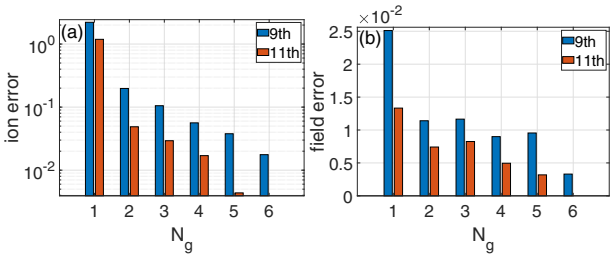

Fig. 3. Error analysis of the Gaussian pulse characterization method for filtered ninth (blue) and 11th harmonics (red): (a) $\mathrm{Error}_{N_g}[P_{\mathrm{ion}}]$ Eq. (9) and (b) $\mathrm{Error}_{N_g}[\tilde{f}]$ Eq. (10).

To characterize the filtered ninth harmonic, we choose a single-color approach in which all Gaussian pulses have the central frequency of the ninth harmonic. The results of the approximations for the time-dependent amplitude $|\tilde{f}(t)|$ (blue) and phase variation $\omega(t)$ (red) using up to six Gaussian pulses (solid lines) are compared in Fig. 2 with the original pulse (dashed lines). The reconstruction with a single Gaussian (a) provides an estimate of the pulse width, but the double-hump structure in the amplitude and the phase variation is, of course, not reproduced. Already inclusion of a second Gaussian pulse (b) provides a significant improvement in this respect; however, the minimum in between the two humps, the small post-pulse structure, and most of the phase variation are still not well reproduced. Using four (c) and six (d) Gaussian pulses, first the main part of the amplitude and then the post-pulse structure and even the phase variation in major parts of the pulse, are well reproduced. We, however, note that using autocorrelation signals, time-independent phases cannot be determined, and a certain pulse cannot be distinguished from the pulse with a time-reversed envelope.

While the results in Fig. 2 visualize the potential of the method, we quantify the convergence by errors for the ionization signal using the objective function as

$$\mathrm{Error}_{N_g}[P_{\mathrm{ion}}] = \sqrt{\int \mathrm{d}\tau\ \mathrm{obj}_{N_g}(\tau)^2}, \tag{9}$$

and the error in the field defined as

$$\mathrm{Error}_{N_g}[\tilde{f}] = \sqrt{\int \mathrm{d}t \left| \tilde{f}_{\mathrm{exact}}(t) - \tilde{f}_{N_g}(t) \right|^2} \tag{10}$$

in Fig. 3. Results for the filtered ninth (blue) and 11th (red) harmonic are compared with each other. In both cases, the error in the ionization signal (a) drops smoothly with an increase in the number of Gaussians included in the method. The number of Gaussians necessary for a similar degree of convergence is smaller for the 11th harmonic, since the pulse envelope (not shown) is less complex than that of the ninth harmonic. The convergence in the error for the ionization signal corresponds to a decrease in the error in the field (b), which reflects the observation in Fig. 2 that the pulse envelope is well reconstructed with a few Gaussians. We note that already two Gaussians are sufficient to provide an estimate of the FWHM pulse duration below 10 a.u. for both harmonics.

After applying the method to isolated ultrashort pulses by filtering the spectrum about a single harmonic, we consider the more complex temporal profile of a pulse train. To this end, we have used a flattop filter to the macroscopic HHG spectrum, where the leading edge is the same Gaussian filter used for the ninth harmonic, and the trailing edge is a Gaussian filter applied to the 11th harmonic. The temporal shape of the resulting pulse train and the autocorrelation signal obtained with the pulse train are shown in Figs. 4(a) and 4(b), respectively.

Since the spectral filtering covers two harmonics, we use a two-color approach with central frequencies equal to those of the ninth and 11th harmonics. A comparison of the original pulse train with the reconstructions shows that one Gaussian pulse per central frequency (c) provides a good approximation, including the duration of the train as well as the duration of the

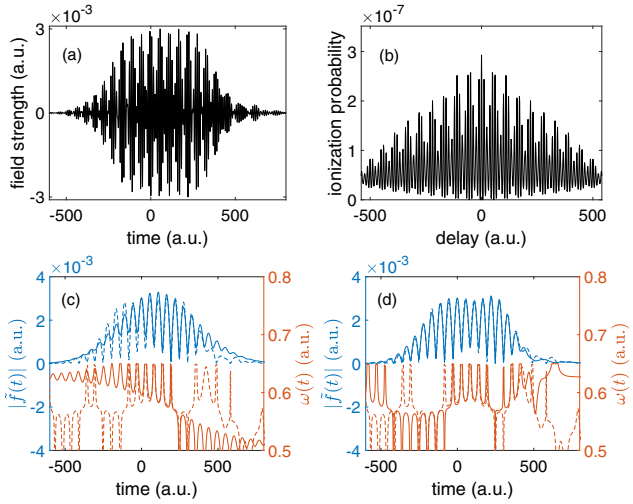

Fig. 4. (a) Temporal profile of the filtered ninth to 11th harmonic spectral range, (b) autocorrelation signal and comparison of time-dependent amplitude (blue) and phase variation (red) of the original pulse (dashed lines) and reconstructions (solid lines) obtained with (c) one and (d) three Gaussians per central frequencies at ninth and 11th harmonics.

individual pulses in the train. However, the envelope with several pulses in the train having similar amplitudes and most of the phase variation are not well reproduced. Using three Gaussian pulses per central frequency (d) improves the agreement with the original pulse significantly.

In summary, using an extension of the two-photon autocorrelation technique based on multiple Gaussian pulses about one or several central frequencies enables a characterization of the amplitude and phase variation of isolated ultrashort pulses and pulse trains. The potential of the method is demonstrated using VUV pulses obtained from numerical simulations of macroscopic high harmonic spectra. The method can be further improved by using alternative basis sets with more parameters or more sophisticated search algorithms in the fitting procedure. The same approach can also be applied to two-photon cross-correlation signals of two isolated ultrashort VUV pulses. The accuracy of the method depends on the determination of one- and two-photon transition dipoles, for which several theoretical methods are available.

Funding. Air Force Office of Scientific Research (FA9550-16-1-0121); National Science Foundation (PHY-1734006).

Acknowledgment. We thank Dr. Jens Biegert for drawing our attention to this topic.

Disclosures. The authors declare no conflicts of interest.

Data Availability. Data underlying the results presented in this paper are not publicly available at this time but may be obtained from the authors upon reasonable request.

REFERENCES

1. M. Galli, V. Wanie, D. P. Lopes, E. P. Månsson, A. Trabattoni, L. Colaizzi, K. Saraswathula, A. Cartella, F. Frassetto, L. Poletto, F. Légaré, S. Stagira, M. Nisoli, R. M. Vázquez, R. Osellame, and F. Calegari, Opt. Lett. **44**, 1308 (2019).
2. J. Reislöhner, C. Leithold, and A. N. Pfeiffer, Opt. Lett. **44**, 1809 (2019).
3. D. E. Couch, D. D. Hickstein, D. D. Hickstein, D. G. Winters, S. J. Backus, S. J. Backus, M. S. Kirchner, S. R. Domingue, J. J. Ramirez, C. G. Durfee, M. M. Murnane, and H. C. Kapteyn, Optica **7**, 832 (2020).
4. A. Stolow, A. E. Bragg, and D. M. Neumark, Chem. Rev. **104**, 1719 (2004).
5. T. Kobayashi and Y. Kida, Phys. Chem. Chem. Phys. **14**, 6200 (2012).
6. S. R. Leone, C. W. McCurdy, J. Burgdörfer, L. S. Cederbaum, Z. Chang, N. Dudovich, J. Feist, C. H. Greene, M. Ivanov, R. Kienberger, U. Keller, M. F. Kling, Z.-H. Loh, T. Pfeifer, A. N. Pfeiffer, R. Santra, K. Schafer, A. Stolow, U. Thumm, and M. J. J. Vrakking, Nat. Photonics **8**, 162 (2014).
7. F. Lépine, M. Y. Ivanov, and M. J. J. Vrakking, Nat. Photonics **8**, 195 (2014).
8. J. L. Ellis, D. D. Hickstein, W. Xiong, F. Dollar, B. B. Palm, K. E. Keister, K. M. Dorney, C. Ding, T. Fan, M. B. Wilker, K. J. Schnitzenbaumer, G. Dukovic, J. L. Jimenez, H. C. Kapteyn, and M. M. Murnane, The J. Phys. Chem. Lett. **7**, 609 (2016).
9. M. Nisoli, P. Decleva, F. Calegari, A. Palacios, and F. Martín, Chem. Rev. **117**, 10760 (2017).
10. R. Borrego-Varillas, L. Ganzer, G. Cerullo, and C. Manzoni, Appl. Sci. **8**, 989 (2018).
11. B. Mignolet, B. F. E. Curchod, F. Remacle, and T. J. Martínez, The J. Phys. Chem. Lett. **10**, 742 (2019).
12. J. Venzke, A. Becker, and A. Jaron-Becker, Phys. Rev. A **103**, 042808 (2021).
13. I. Orfanos, I. Makos, I. Liontos, E. Skantzakis, B. Förg, D. Charalambidis, and P. Tzallas, APL Photonics **4**, 080901 (2019).
14. P. M. Paul, E. S. Toma, P. Breger, G. Mullot, F. Augé, P. Balcou, H. G. Muller, and P. Agostini, Science **292**, 1689 (2001).
15. J. Itatani, F. Quéré, G. L. Yudin, M. Y. Ivanov, F. Krausz, and P. B. Corkum, Phys. Rev. Lett. **88**, 173903 (2002).
16. Y. Mairesse and F. Quéré, Phys. Rev. A **71**, 011401 (2005).
17. S. A. Trushin, K. Kosma, W. Fuß, and W. E. Schmid, Opt. Lett. **32**, 2432 (2007).
18. M. Chini, S. Gilbertson, S. D. Khan, and Z. Chang, Opt. Express **18**, 13006 (2010).
19. V. Gruson, L. Barreau, Á. Jiménez-Galan, F. Risoud, J. Caillat, A. Maquet, B. Carré, F. Lepetit, J.-F. Hergott, T. Ruchon, L. Argenti, R. Taïeb, F. Martín, and P. Salières, Science **354**, 734 (2016).
20. P. Tzallas, D. Charalambidis, N. A. Papadogiannis, K. Witte, and G. D. Tsakiris, Nature **426**, 267 (2003).
21. Y. Nabekawa, T. Shimizu, T. Okino, K. Furusawa, H. Hasegawa, K. Yamanouchi, and K. Midorikawa, Phys. Rev. Lett. **96**, 083901 (2006).
22. K. Midorikawa, Y. Nabekawa, and A. Suda, Prog. Quantum Electron. **32**, 43 (2008).
23. F. Reiter, U. Graf, M. Schultze, W. Schweinberger, H. Schröder, N. Karpowicz, A. M. Azzeer, R. Kienberger, F. Krausz, and E. Goulielmakis, Opt. Lett. **35**, 2248 (2010).
24. P. Tzallas, E. Skantzakis, L. A. A. Nikolopoulos, G. D. Tsakiris, and D. Charalambidis, Nat. Phys. **7**, 781 (2011).
25. K. L. Ishikawa and K. Ueda, Appl. Sci. **3**, 189 (2013).
26. A. Cuyt, V. Petersen, B. Verdonk, H. Waadeland, and W. Jones, *Handbook of Continued Fractions for Special Functions* (Springer, 2008).
27. S. Winitzki, in *International Conference on Computational Science and its Applications* (Springer, 2003), pp. 780–789.
28. R. Reiff, J. Venzke, A. Jaron-Becker, and A. Becker, OSA Continuum **4**, 1897 (2021).
29. J. Venzke, A. Jaroń-Becker, and A. Becker, J. Phys. B: At. Mol. Opt. Phys. **53**, 085602 (2020).
30. C. Hernández-García, J. A. Pérez-Hernández, J. Ramos, E. C. Jarque, L. Roso, and L. Plaja, Phys. Rev. A **82**, 033432 (2010).
31. R. Reiff, T. Joyce, A. Jaron-Becker, and A. Becker, J. Phys. Commun. **4**, 065011 (2020).